Cross sections for one-neutron knock-out from ^{37}Ca at intermediate energy

A. Bürger,[1,2,*] F. Azaiez,[3] A. Algora,[4] A. Al-Khatib,[1] B. Bastin,[5] G. Benzoni,[6] R. Borcea,[7] C. Bourgeois,[3] P. Bringel,[1] E. Clément,[2] J.-C. Dalouzy,[8] Z. Dlouhý,[9] Z. Dombrádi,[4] A. Drouart,[2] C. Engelhardt,[1] S. Franchoo,[3] Z. Fülöp,[4] A. Görgen,[2] S. Grévy,[8] H. Hübel,[1] F. Ibrahim,[3] W. Korten,[2] J. Mrázek,[9] A. Navin,[8] F. Rotaru,[7] P. Roussel Chomaz,[8] M.-G. Saint-Laurent,[8] G. Sletten,[10] D. Sohler,[4] O. Sorlin,[8] M. Stanoiu,[7] I. Stefan,[8] C. Theisen,[2] C. Timis,[11] D. Verney,[3] and S. Williams[11]

[1]*Helmholtz-Institut für Strahlen- und Kernphysik, Universität Bonn, Nußallee 14-16, D-53115 Bonn, Germany*
[2]*CEA Saclay, IRFU/Service de Physique Nucléaire, F-91191 Gif-sur-Yvette, France*
[3]*Institut de Physique Nucléaire, IN2P3-CNRS, F-91406 Orsay, France*
[4]*Institute of Nuclear Research, P.O. Box 51, H-4001 Debrecen, Hungary*
[5]*Laboratoire de Physique Corpusculaire, 6 Boulevard Maréchal Juin, F-14050 Caen, France*
[6]*INFN Sezione di Milano, via Celoria 16, I-20133 Milano, Italy*
[7]*Institute of Atomic Physics IFIN-HH, Bucharest-Magurele, P.O. Box MG-6, Bucharest-Magurele, Romania*
[8]*GANIL, Boulevard Henri Becquerel, BP 55027, F-14076 Caen, France*
[9]*Nuclear Physics Institute of ASCR, CZ-250 68 Řež, Czech Republic*
[10]*Niels Bohr Institutet, Københavns Universitet, Blegdamsvej 17, DK-2100 København Ø, Denmark*
[11]*Department of Physics, University of Surrey, Guildford GU2 7XH, Surrey, United Kingdom*

(Received 12 September 2011; revised manuscript received 17 November 2012; published 26 December 2012)

The cross section for the knock-out of a deeply bound valence neutron from ^{37}Ca at an incident beam energy of 60A MeV has been measured along with momentum distributions of the residual nuclei and γ rays from the de-excitation of the first excited state in ^{36}Ca. As for other cases of deeply bound nucleons studied using knock-out reactions, the reduction of the measured cross section compared to theoretical predictions is stronger than those observed for near-magic stable nuclei. Both the momentum distributions and the excitation energy of the first excited state in ^{36}Ca indicate a sizable $N = 16$ gap.

DOI: 10.1103/PhysRevC.86.064609 PACS number(s): 25.60.Gc, 23.20.Lv, 27.30.+t

I. INTRODUCTION

The nuclear shell model makes detailed predictions about the mixing of configurations forming individual states in a nucleus. The relation between two states can be expressed by means of the spectroscopic factor (SF). For a reaction where one nucleon is removed from a nucleus with A nucleons, the SF describes the parentage of the initial state of the nucleus A for the final state in the product (with $A - 1$ nucleons) coupled to a single nucleon with specific quantum numbers. Spectroscopic factors can be calculated within the shell model, and they can also be obtained from experiment. Within the shell model, configuration mixings are calculated for the initial and final states, and SFs are derived from the overlap of wave functions. An experimental SF may be determined from the ratio of a measured cross section and a theoretical single-particle cross section. For the calculation of the single-particle cross sections, a reaction model must be used and, consequently, the experimental SF contains a model dependence.

For nuclei close to the drip lines and with deeply or loosely bound nucleons, knock-out reactions with radioactive isotope beams of intermediate energies allow one to measure the SFs [1]. The single-particle cross sections are in this case often calculated using an eikonal approximation for the reaction. Experiments show that, for most nuclei near the valley of stability, SFs measured using knock-out reactions or electron scattering are smaller than the value predicted by shell-model calculations. This reduction can be expressed by using the ratio of experimental and theoretical cross sections, $R_s = \sigma_{\mathrm{exp}}/\sigma_{\mathrm{th}}$, which equals the ratio of SFs except for a center-of-mass correction [1,2]. When using knock-out reactions or electron scattering, typical values of R_s are around 0.6–0.7 for near-stable nuclei [3].

In previous knock-out studies of deeply bound valence neutron states, the $1d_{5/2}$ and $2s_{1/2}$ states in ^{32}Ar and ^{34}Ar, respectively, significantly smaller R_s values have been reported [2,4]. Experimental data from knock-out reactions and electron scattering indicate a systematic correlation between R_s and the difference in nucleon separation energy, ΔS, taken as $S_n - S_p$ and $S_p - S_n$ for neutron and proton knock-out, respectively [3]. In this study, R_s may be close to 1 for removing nucleons of the weakly bound species, while R_s values down to 0.24 are measured for the removal of nucleons of the strongly bound species. For the latter case, it is suggested that the large quenching is due to correlation effects linked to the high nucleon separation energy. However, in Ref. [5] an analysis of SFs measured in (p, d) and (d, p) transfer reactions was made for a range of nuclei with neutron separation energies S_n from 0.5 to 19 MeV, and no systematic quenching of the SFs as a function of S_n was observed. This observation was confirmed in a study of, among others, ^{34}Ar, using (p, d) transfer reactions in inverse kinematics [6]. Here, also indications for a dependence of the quenching on the optical model potential used in the calculations have been found. An explanation for the dependence of the quenching on ΔS for oxygen isotopes has recently been proposed [7], where the

*Present address: Meteorologisk Institutt, Postboks 43, Blindern, N-0313 Oslo, Norway; alexander.buerger@met.no

SFs are calculated using an *ab initio* coupled-cluster approach including continuum states. A different direction has been taken by other authors, relying instead on a intranuclear-cascade model [8].

The quenching observed in knock-out reactions may be tested by measuring SFs in deeply bound nuclei near doubly closed shells. In such nuclei, one can expect an enhanced single-particle character and, subsequently, an increased reliability of shell-model predictions, reducing one possible source of uncertainty. The focus of the present work is on the one-neutron knock-out from ^{37}Ca, producing ^{36}Ca at an average, mid-target beam energy of 50A MeV. The nucleon binding energies of ^{37}Ca are $S_n = 14.8$ MeV and $S_p = 3.0$ MeV ($\Delta S = 11.8$ MeV) [9]. Both nuclei have a closed shell at $Z = 20$, and, as in the mirror nuclei ^{36}S and ^{37}Cl, a large $N = 16$ gap may be expected with a rather pure single-particle character of the low-lying states.

II. EXPERIMENTAL SETUP

The experiment was performed at GANIL. The two-step fragmentation technique was used to produce ^{36}Ca ions. A primary beam of ^{40}Ca with an energy of 95A MeV was fragmented on a 400 mg/cm^2 carbon foil in the SISSI target device [10]. The resulting beam cocktail was then purified using the α spectrometer with a 521 μm Al degrader, optimized for ^{37}Ca fragments. The beam reached the secondary ^{9}Be target of 198(10) mg/cm^2 thickness with an energy of 60A MeV (for ^{37}Ca). After the secondary target, the beamlike particles emerge with energies around 38A MeV (for ^{37}Ca) and enter the SPEG spectrometer [11]. A slit to catch ions with high $B\rho$ was placed in SPEG to stop most of the secondary ^{37}Ca beam before it reaches the focal plane detectors.

An identification of the secondary beam particles was obtained for each event from the time difference between the high frequency (HF) of the cyclotron and the signal from a particle detector placed 1.5 m in front of the beryllium target. SPEG was used to identify the reaction products and to measure their momenta. The time of flight between the particle detector in front of the secondary target and the scintillator stopping the beam at the end of SPEG was recorded for each event. Together with the magnetic rigidity measurement, an A/Q identification was obtained. The Z identification was provided by the energy losses measured in the ionization chambers of SPEG. The total energy deposited in the beam-stopping scintillator provided a secondary A/Q identification, and the energy losses in the drift chambers gave a secondary Z identification. Events were selected for further analysis only if both A/Q and both Z identifications agreed. Figure 1 demonstrates that the particle identification after the secondary target allowed for an unambiguous selection of ^{36}Ca events.

Gamma-ray energies were measured with the Château de Cristal, an array of 74 BaF_2 detectors [12], that surrounded the beryllium target. The γ-ray detectors were calibrated using a ^{22}Na source and known transitions in the nuclei ^{28}Si, ^{32}S, ^{34}Ar, ^{29}Si, and ^{33}Cl. Excited states in these nuclei were produced in the secondary target from different beam components. The detection efficiency of the Château de Cristal at energies up to

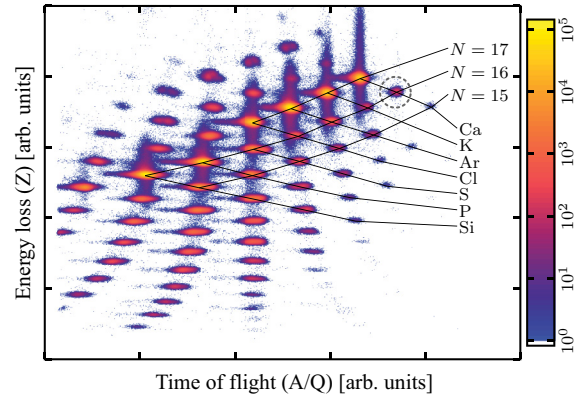

FIG. 1. (Color online) Particle identification matrix in the focal plane of SPEG, without selection of the secondary beam component. The nucleus ^{36}Ca (encircled) is clearly separated from other nuclei.

1.3 MeV was determined using ^{60}Co and ^{152}Eu sources. Using a GEANT-4 [13] simulation, efficiencies were then extrapolated to higher γ-ray energies. While the agreement between the simulated and measured efficiencies is better than 2%, we have included in the calculations an estimated uncertainty of 5% for efficiencies that are extrapolated to 3 MeV. An add-back procedure was applied to improve the peak-to-total ratio. The Doppler correction of γ-ray energies from in-flight decays employed the momentum measured in SPEG. The lifetime of the 2^+_1 state in ^{36}S is 75(20) fs [14], but for ^{36}Ca, the corresponding lifetime is unknown. If the lifetime was twice as large as in ^{36}S, the mean flight path before decay would be only $\approx 2\%$ of the target thickness, so that stopping effects are neglected. As the calculated knock-out cross sections depend only weakly on the projectile energy, it was assumed that the γ rays were emitted in the center of the beryllium target.

III. EXPERIMENTAL RESULTS

The total γ-ray energy spectrum obtained for ^{36}Ca is shown in Fig. 2. The energy of the 2^+ state in ^{36}Ca was determined to be $E(2^+) = 3036(11)$ keV. The given uncertainty value

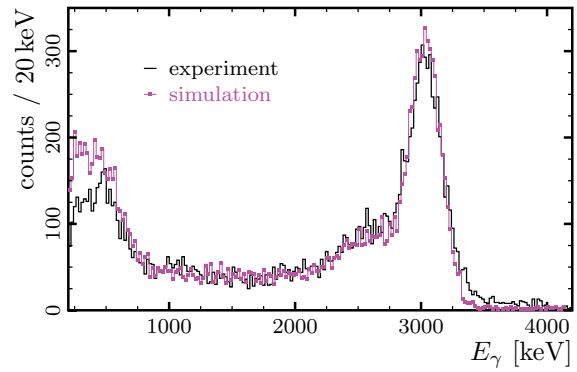

FIG. 2. (Color online) Comparison of experimental (black line) and simulated (magenta squares) Doppler-corrected γ-ray energy spectra for ^{36}Ca.

includes the calibration and the peak fit uncertainties. The excitation energy obtained in this experiment is in agreement with the value of $E(2^+) = 3015(16)$ keV measured at GSI [15]. Figure 2 includes a simulation of the emission of a single γ ray of 3036 keV from ^{36}Ca. Given the good agreement of the two spectra, we conclude that no other states decaying by γ-ray emission were populated and that all γ-ray energies between 1.2 and 3.3 MeV originated from the decay of the 2^+ state. From the simulation, the efficiency of the Château de Cristal for measuring either full absorption or a Compton escape with $E_\gamma \geqslant 1.2$ MeV is 35%.

The total momentum distribution for the detected ^{36}Ca nuclei was measured by using SPEG. The 7% momentum bite of SPEG (the part that is common over two sets of our measurements) runs from 9260 to 9860 MeV/c. Within this range, acceptance corrections are not necessary [11]. The part of the distribution that is in coincidence with a γ ray was scaled by the detection efficiency to obtain the momentum distribution for the 2^+ state. As no other excited states are populated, the ground-state momentum distribution is then the difference between the total and 2^+-state distributions.

IV. DISCUSSION

The knock-out code MOMDIS [16] was used for the calculation of single-particle cross-sections as well as parallel and transverse momentum distributions. A Woods-Saxon potential was parametrized with a diffuseness of 0.7 fm. The potential depth V_0 and radius r_0 were adjusted for both the ground state and the 2^+ state to reproduce the effective separation energy $-E = S_n + E_x$ and the rms core-neutron separation $r_{\rm rms} = \sqrt{A/(A-1)}r_{\rm HF}$ [1,17], where $r_{\rm HF}$ was calculated alternatively with a SLy4 [18] and a SkX Skyrme force [19]. The spin-orbit parameters were chosen as $V_{\rm so} = -7$ MeV for its strength, $r_{\rm so} = A^{1/3}$ fm $= 3.3$ fm for its radius and $a_{\rm so} = 0.7$ fm for its diffuseness. The result of the Woods-Saxon parametrization is given in Table I. For the beryllium target nuclei, a Gaussian matter distribution with a radius of 2.36 fm, modulated with Z_t/A_t for protons and N_t/A_t for neutrons, was assumed [4,16]. The density distribution of the core was calculated in a Hartree-Fock approach for protons and neutrons separately, first with a SLy4 and then a SkX force. The radius of the residue equals $r_{\rm HF} = 3.31$ fm for SLy4 and 3.29 fm for the SkX parametrization [20].

The comparison of experimental and calculated momentum distributions requires that the different energy losses of ^{36}Ca and ^{37}Ca ions in the target be taken into account. A Monte Carlo simulation of the knock-out reaction was used for this purpose. Momentum distributions parallel and perpendicular to the direction of the incoming particle were obtained with MOMDIS for a set of laboratory energies as the beam particle passes through the target. These distributions were interpolated and sampled according to the energies of the particles at the reaction point in the beryllium target, taking into account the energy loss of the ion.

TABLE I. V_0 and r_0 parameters for the SLy4 and SkX forces used in the Momdis cross section and momentum distribution calculations that allow one to obtain the separation energy $-E = S_n + E_x$ and core-neutron separation $r_{\rm rms}$.

	Force	V_0 (MeV)	r_0 (fm)	E (MeV)	$r_{\rm rms}$ (fm)
$1d_{3/2}$	SLy4	−59.1	3.88	−14.8	3.36
$2s_{1/2}$	SLy4	−61.5	3.95	−17.8	3.36
$1d_{3/2}$	SkX	−61.7	3.76	−14.8	3.29
$2s_{1/2}$	SkX	−64.8	3.78	−17.8	3.29

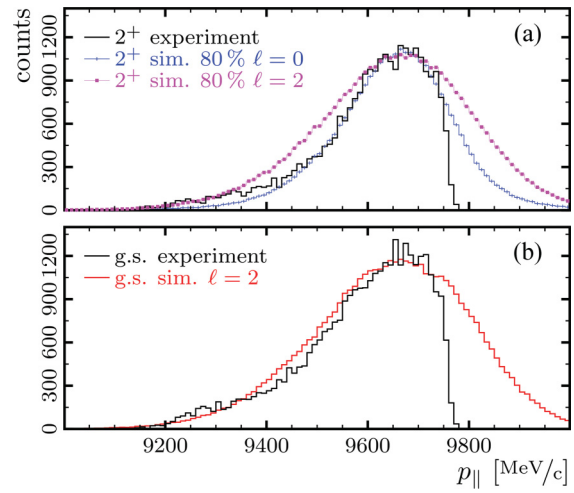

FIG. 3. (Color online) Comparison of experimental (black line) and simulated momentum distributions after one-neutron knock-out from ^{37}Ca, leading to the 2^+ excited state in ^{36}Ca (a) and to the ground state of ^{36}Ca (b). At high momenta, the experimental spectra are cut by the slit in SPEG. The simulated distribution for the 2^+ state with a ratio ($\ell = 0$:$\ell = 2$) = 80:20 is shown in blue, the combination ($\ell = 0$:$\ell = 2$) = 20:80 in magenta, and the $\ell = 2$ simulation for the ground state in red. See text for details.

The experimental momentum distributions for the ground state and the excited 2^+ state in ^{36}Ca are compared to simulated $\ell = 0$ and $\ell = 2$ momentum distributions in Fig. 3. It has been observed in other experiments that the distributions at low momenta are affected by deviations from eikonal theory [21–23]. Energy-threshold effects have been seen to cause a steep cutoff at the higher end of the parallel momentum distributions, while dissipative processes and nucleon-removal dynamics have been shown to induce a low-momentum tail especially for large values of ℓ. At our beam energy of 60A MeV, the high-energy cutoff is expected to occur at about 9780 MeV/c. The presence of a slit in SPEG, necessary to suppress the scattered primary beam, prevents us from making any further statement on this. As explained above, the momentum acceptance of SPEG of 7% would affect the measured distributions below 9260 MeV/c. The low-momentum tail therefore cannot be reliably considered. To exclude any possible distortions, the fit of the momentum distribution only covers the range from 9500 to 9740 MeV/c.

We find that the experimental distribution for the ground state, for which only $\ell = 2$ is allowed, is slightly narrower than the simulated one. For the excited 2^+ state, a χ^2 value of 1.43 is obtained for a ratio of 80% of $\ell = 0$ to 20% of $\ell = 2$. Figure 4 shows the behavior of this χ^2 as a function of the

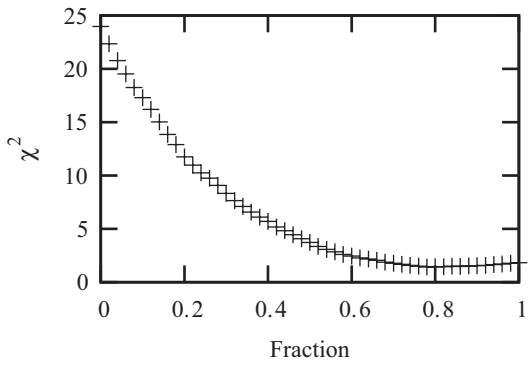

FIG. 4. Dependence of χ^2 of the fitted momentum distribution after one-neutron knock-out from ^{37}Ca, leading to the 2^+ excited state in ^{36}Ca, on the fraction of $\ell = 0$ it contains. See text for details.

$\ell = 0$ fraction. The fit itself agrees well with the data over the fitting range but, due to the excess momentum spread in the simulation that we mentioned, the actual $\ell = 0$ contribution might be slightly lower. If the momentum range is extended to lower values, the χ^2 value deteriorates rapidly. The χ^2 minimization yields an uncertainty of around 20% for the ℓ contributions, excluding systematic errors in the calculated energy-loss difference of ^{36}Ca and ^{37}Ca in the beryllium target. Even though the binding energy of 15 MeV of the ejected neutron is not negligible compared to the energy of the beam of 60A MeV, slowing down to 38A MeV when it passes through the target, the agreement of the calculated momentum distribution with the data warrants the eikonal approximation of the reaction model.

Our data show a distribution that is narrower than the fit based on the simulation. The absence of a dissipative tail at low momentum in our data can be compared to data reported in the literature [2]. The neutron knock-out on ^{32}S, ^{33}Cl, and ^{34}Ar to the ground state in the final nucleus did not show a significant tail till the distribution had dropped to about 1/4 of its maximum height. In these three cases, the ratio of nucleon separation energy to beam energy per nucleon is not far from our case. We may thus possibly expect a deviation from a Gaussian profile at the leftmost range of our measurement while, for the bigger part of the distribution, the absence of a significant tail indicates that the eikonal approximation is appropriate.

To determine cross sections for the production of ^{36}Ca, the momentum distributions were integrated and extrapolated beyond the SPEG slit. For this extrapolation, the ratio between the integrals of the simulated (without slit) and experimental (with slit) momentum distributions was used. A 15% uncertainty for the extrapolation area was included to account for uncertainties stemming from the width of the distributions as discussed above. The total cross section was then determined in two ways. The first technique was to select a time-difference window corresponding to ^{37}Ca between the cyclotron HF and the particle detector just in front of the target, and then to count the incoming ^{37}Ca ions with a scaled-down particle trigger on this detector. The ^{36}Ca ion count was determined from the extrapolated SPEG momentum distributions. This method yields a cross section for the production of ^{36}Ca of 5.4(5) mb. The second method makes use of a calibration run from just before the start of the ^{36}Ca production runs. In this run, the beam intensity was reduced, the SPEG slit removed, and the $B\rho$ of SPEG adjusted for ^{37}Ca. Therefore, the ^{37}Ca ions could be counted with SPEG, and, by assuming that the beam composition did not change with the intensity increase, the cross section can be calculated from the ratio of ^{36,37}Ca to the total number of beam particles, counted by a scaler. With this method, a production cross section of 5.8(5) mb was obtained. Both values agree within uncertainties, and the average of 5.6(5) mb for the production of ^{36}Ca is adopted. This cross section does not account for the possible decay of the 2^+ state in ^{36}Ca by proton emission. The proton separation energy S_p is only 2.56(4) MeV [9]. Proton emission cannot be detected with the present experimental setup, and the measured total cross section has to be considered as a lower limit. The branching ratio B for populating the two final states was obtained from the ratio of integrals of the extrapolated momentum distributions. The branching ratio was then used to calculate the partial cross sections and the SF.

Single-particle cross sections $\sigma_{\rm sp}$ were calculated with MOMDIS for a mid-target energy of 50A MeV. Theoretical spectroscopic factors $C^2S_{\rm th}$ were calculated with the code ANTOINE [24,25] by taking the USD interaction [26]. When using the modified interactions USDm and USDm^2 described in [15], where the single-particle energies are directly taken from excited states in the mirror nuclei ^{17}O and ^{17}F to reproduce explicitly the mirror energy differences in ^{36}Ca-^{36}S and ^{32}Ar-^{32}Si, respectively, or otherwise the updated USDB interaction [27], the calculated spectroscopic factors vary from 0.91 to 0.94 for the ground state and from 1.10 to 1.16 for the excited state, the USD values being in the middle with 0.92 and 1.13.

The theoretical cross section $\sigma_{\rm th}$ is the product of $\sigma_{\rm sp}$, $C^2S_{\rm th}$, and a center-of-mass correction term [28]. The branching ratios, cross sections, and spectroscopic factors are summarized and compared to the theoretical values in Table II. The uncertainties given for the experimental cross sections are dominated by the statistical errors, in particular 24% due the subtraction of the excited state in case of the ground state, to which is added 5% for the target thickness and 5% for the beam identification, followed by smaller contributions from particle-detector efficiencies and estimated uncertainties for the simulation-based extrapolations. For the single-particle cross sections and the derived experimental SF, neither the uncertainty from the choice of parameters for the knock-out reaction calculation with MOMDIS nor uncertainties in the radius stemming from the parameter choice in the Hartree-Fock calculation were taken into account.

The calculated cross section for the ground state amounts to $\sigma_{\rm th} = 9.04$ mb for SLy4 and 8.93 mb for SkX. Including the effects from Pauli blocking in the MOMDIS code [16,29] increases the cross sections by 3% and one obtains $\sigma_{\rm th} =$ 9.30mb for SLy4 and 9.18mb for SkX. The latter values result in a reduction factor, defined as the ratio of the experimental and theoretical cross sections, of $R_s = 0.34(7)$ or 0.35(8) for SLy4 or SkX, respectively. We may conclude that the choice of interaction that was used to calculate the density distributions has little effect on the final result. At

TABLE II. Branching ratios B and measured partial cross sections σ_{exp} extracted from the momentum distributions of ^{36}Ca in comparison with theoretical single-particle cross sections σ_{sp}, spectroscopic factors C^2S_{th}, and theoretical cross sections σ_{th}. Pauli blocking was applied for the calculation of the cross sections, with the SLy4 and SkX forces.

State	E_x(keV)	$n\ell j$	B(%)	σ_{exp}(mb)	σ_{sp}(mb)	C^2S_{th}	lσ_{th}(mb)	R_s	Force
0^+	0	$1d_{3/2}$	57(11)	3.2(7)	9.57	0.92	9.30	0.34(7)	SLy4
					9.45		9.18	0.35(8)	SkX
2^+	3036(11)	$2s_{1/2}$	43(11)	2.4(6)[a]	11.6	1.13	13.9	0.17(5)[a]	SLy4
					11.4		13.6	0.18(5)	SkX

[a]Lower limit assuming no proton emission; see text.

$\Delta S = 11.8$ MeV, our R_s value fits well into the systematics given by Gade *et al.* [3].

For the excited 2^+ state, we compute a theoretical cross section with Pauli blocking of $\sigma_{th} = 13.9$ mb for SLy4 or 13.6mb for SkX. The reduction factor obtained, $R_s = 0.17(5)$ or 0.18(5), is unusually low. Because, as mentioned above, proton emission could not be detected, and as the branching ratio between the γ and proton channels is not known, the actual number of ^{36}Ca ions produced in the 2^+ state cannot be determined. As E_x exceeds S_p by about 0.5 MeV, proton emission must be expected and we assume that unobserved proton emission is the reason for the small R_s value. Therefore, our R_s value for the 2^+ state represents only a lower limit.

V. CONCLUSION

The high excitation energy of the 2^+ state of more than 3 MeV establishes a large $N = 16$ shell gap and points toward rather pure configurations of the ground and the 2^+ state in ^{36}Ca. Shell-model calculations with the USD interaction predict pure s and d configurations for the ground and excited states, respectively, where admixtures of other configurations only sum up to about 10%. The width of the measured momentum distributions, relying on a pure $\ell = 2$ character for the ground state and a fitted mixture of ($\ell = 0$:$\ell = 2$) = 80:20 for the excited 2^+ state, agrees well with these calculations and is experimental support for the existence of a large $N = 16$ neutron subshell gap in ^{36}Ca similar to the proton $Z = 16$ subshell gap in ^{36}S.

Our measured reduction factor for the ground state of a doubly closed shell nucleus with deeply bound valence neutrons falls within the systematics for other nuclei with deeply bound nucleons that have been studied in knock-out reactions. It could be interesting to compare this result with coupled-cluster calculations, which recently have been able to move up to the calcium isotopes [7,30].

ACKNOWLEDGMENTS

We wish to thank the accelerator staff of GANIL and the SPEG technical staff for their support during the experiment. We acknowledge the support from the European Community through the Eurons project Contract No. RII3-CT-2004-506065, from BMBF Germany, No. 06 BN 109, from OTKA Hungary, No. K100835 and No. NN104543, and from the Bolyai Janos Foundation.

[1] P. G. Hansen and J. A. Tostevin, Annu. Rev. Nucl. Part. Sci. **53**, 219 (2003).
[2] A. Gade *et al.*, Phys. Rev. C **69**, 034311 (2004).
[3] A. Gade *et al.*, Phys. Rev. C **77**, 044306 (2008).
[4] A. Gade *et al.*, Phys. Rev. Lett. **93**, 042501 (2004).
[5] J. Lee, M. B. Tsang, and W. G. Lynch, Phys. Rev. C **75**, 064320 (2007).
[6] J. Lee *et al.*, Phys. Rev. Lett. **104**, 112701 (2010).
[7] Ø. Jensen, G. Hagen, M. Hjorth-Jensen, B. A. Brown, and A. Gade, Phys. Rev. Lett. **107**, 032501 (2011).
[8] C. Louchart, A. Obertelli, A. Boudard, and F. Flavigny, Phys. Rev. C **83**, 011601(R) (2011).
[9] G. Audi, A. Wapstra, and C. Thibault, Nucl. Phys. A **729**, 337 (2003).
[10] E. Baron, J. Gillet, and M. Ozille, Nucl. Instrum. Methods A **362**, 90 (1995).
[11] L. Bianchi *et al.*, Nucl. Instrum. Methods A **276**, 509 (1989).
[12] F. A. Beck, in *Instrumentation for Heavy Ion Nuclear Research*, Nuclear Science Research Conference Series, Vol. 7, edited by D. Shapira (Harwood Academic Publishers, New York, 1984), p. 129.
[13] S. Agostinelli *et al.*, Nucl. Instrum. Methods A **506**, 250 (2003); http://geant4.web.cern.ch/geant4/.
[14] ENSDF Database, http://www.nndc.bnl.gov/ensdf/.
[15] P. Doornenbal *et al.*, Phys. Lett. B **647**, 237 (2007).
[16] C. A. Bertulani and A. Gade, Comput. Phys. Commun. **175**, 372 (2006).
[17] A. Gade *et al.*, Phys. Rev. C **74**, 047302 (2006).
[18] E. Chabanat *et al.*, Nucl. Phys. A **635**, 231 (1998).
[19] B. A. Brown, Phys. Rev. C **58**, 220 (1998).
[20] E. Khan (private communication).
[21] J. Tostevin *et al.*, Phys. Rev. C **66**, 024607 (2002).
[22] A. Gade *et al.*, Phys. Rev. C **71**, 051301(R) (2005).
[23] F. Flavigny, A. Obertelli, A. Bonaccorso, G. F. Grinyer, C. Louchart, L. Nalpas, and A. Signoracci, Phys. Rev. Lett. **108**, 252501 (2012).
[24] E. Caurier, Shell Model Code ANTOINE, IReS, Strasbourg, France, http://sbgat194.in2p3.fr/theory/antoine/menu.html, 1989–2004.
[25] E. Caurier and F. Nowacki, Acta Phys. Pol. B **30**, 705 (1999).
[26] B. Wildenthal, Progr. Nucl. Part. Phys. **11**, 5 (1984).
[27] B. A. Brown and W. A. Richter, Phys. Rev. C **74**, 034315 (2006).
[28] A. Dieperink and T. de Forest, Jr., Phys. Rev. C **10**, 543 (1974).
[29] M. Hussein, R. Rego, and C. Bertulani, Phys. Rep. **201**, 279 (1991).
[30] G. Hagen, M. Hjorth-Jensen, G. R. Jansen, R. Machleidt, and T. Papenbrock, Phys. Rev. Lett. **109**, 032502 (2012).